

YbPO₄ crystals in as-drawn silica-based optical fibers

Zhuorui Lu^{1,2,0}, Natalia Vakula^{3,0}, Michèle Ude¹, Martiane Cabié⁴, Thomas Neisius⁴, François Orange⁵, Franck Pigeonneau², Laetitia Petit³, Wilfried Blanc^{1,*}

1. Université Côte d'Azur, Institut de Physique de Nice, CNRS UMR7010, Nice, France

2. MINES Paris, PSL Research University, CEMEF - Centre for material forming, CNRS UMR 7635, CS 10207, rue Claude Daunesse 06904 Sophia Antipolis Cedex, France

3. Photonics Laboratory, Tampere University, Korkeakoulunkatu 3, 33720 Tampere, Finland

4. Aix Marseille Univ, CNRS, Centrale Marseille, FSCM, CP2M, 13397 Marseille, France

5. Université Côte d'Azur, CCMA, Nice, France

*Corresponding author: wilfried.blanc@inphyni.cnrs.fr

⁰ Co-shared first authorship

Highlights

(1) YbPO₄ crystals are prepared by precipitation from aqueous solution

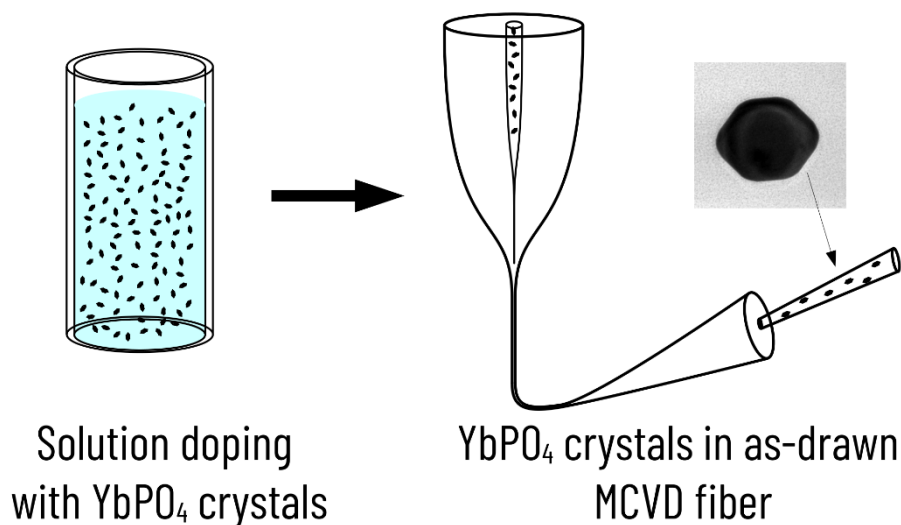
(2) YbPO₄ crystals survive all along the MCVD process and the fiber drawing step

(3) YbPO₄ crystals are aligned during the fiber drawing

Abstract

MCVD germanosilica glass embedded with YbPO₄ crystals were for the first time drawn into optical fibers. Solution doping was used to embed the crystals in the silica soot prior to the collapsing step. We demonstrate, using scanning/transmission electron microscopes and confocal Raman microscope, that YbPO₄ crystals survive not only the MCVD process but also the drawing process despite the high temperature involved (up to 2100 °C) during fabrication processes. The fiber contains 100 nm-crystals with the same composition and structure as the as-prepared crystals. During the drawing process, these crystals tend to have a preferential orientation of their c-axis along the drawing direction. These results open a new route to fabricate glass-based composite fibers containing crystalline particles without additional post heat-treatment.

Graphical abstract



Keywords

Chemical vapor deposition, scanning electron microscopy, transmission electron microscopy, silica, fiber

1. Introduction

Optical fibers containing nanoparticles have been of growing interest in recent years for applications as lasers, amplifiers or sensors [1]. In the context of sensors (temperature, stress, biology, etc.), the properties sought are related to the scattering of light induced by the presence of nanoparticles. The principle of detection is based either on the analysis of the backscattered light measured by Optical Backscatter Reflectometry (OBR) or on the measurement of the intensity ratio between the transmitted and the reflected light [2-3]. In the context of lasers and amplifiers, nanoparticles are sought to encapsulate luminescent ions (rare-earth ions or transition metals) [4-5]. This approach allows to design a chemical and structural environment different from the host glass leading to modified emission characteristics, based on the luminescent ion environment.

These applications depend on our ability to control the characteristics (composition, structure, size, etc.) of the nanoparticles in the fiber. To achieve this goal, several fabrication processes are studied. One usual approach is based on the Modified Chemical Vapor Deposition (MCVD) process commonly used in industry to prepare specialty optical fibers (lasers, sensors, etc.). During the solution doping step, ions such as alkaline earths ions can be added to form nanoparticles via phase separation mechanisms [6]. Such nanoparticles are amorphous in the as-drawn fiber.

The formation of crystalline particles in the fiber is of particular interest because a crystalline structure can increase the absorption and emission cross sections of rare-earth ions or make transition metals optically active. To obtain crystals, one manufacturing process can be based on the thermal treatment of the MCVD preform prior to drawing the fiber [7]. However, the most common process used to obtain crystals is based on the post heat treatment of the fiber [8]. As in the preparation of a glass-ceramic, the choice of temperature and treatment durations allows one to control the nucleation and growth of the particles. However, this approach has drawbacks such as the length of the treated fiber, mechanical embrittlement, the need to strip the fiber and then recoat it after the heat treatment. In order to avoid these drawbacks, it is sought to obtain homogeneously dispersed crystalline particles directly in the as-drawn fiber. To reach this goal, targeted crystals could be embedded in the glass matrix. This approach is however limited because it requires maintaining the integrity of the particles throughout the process. Indeed, it has been reported that corrosive effect of the glass matrix and high temperature tend to degrade nanoparticles [9-11]. By controlling the melting condition, it was demonstrated that it is possible to limit the corrosive effect of the glass matrix [12] and composite phosphate fibers were successfully drawn into fibers [13].

Crystal of interest in this study is YbPO_4 . Such crystals were observed in a glass rod drawn in a 1.6 mm cane [14]. In this report, YbPO_4 crystalline nanoparticles were obtained through phase separation mechanisms. Here, we are interested in an alternative route of fabrication based on the doping with YbPO_4 crystals. Recently, YbPO_4 crystals were successfully embedded in glasses prepared using standard melting process [15]. These crystals were found to maintain their integrity in glasses with low glass transition temperature [15]. As these crystals possess high temperature stability (melting temperature is 2150°C) and chemical durability [16,17], these crystals are promising candidates to use for the fabrication of composite fibers from silica glass matrix typically prepared at temperature larger than 2000°C .

In this paper, we report the preparation of composite fiber using solution doping to embed the YbPO_4 crystalline particles in the silica network. We demonstrate, for the first time, the presence of such crystalline particles in the as-drawn fiber with the same composition and structure as the crystalline particles used as dopant. We demonstrate here that doping with these crystals using the industrial MCVD process allows to obtain YbPO_4 crystals in the as-drawn silica-based fiber.

2. Experimentals

2.1. Fiber preparation

The preform was prepared by using the MCVD process. The starting tube is a F300 silica tube from Heraeus (Germany) with outer and inner diameters of 20 and 17 mm, respectively. A porous GeO₂-doped silica core layer was deposited inside the tube. The doping solution was prepared by suspending 4.6 g of YbPO₄ nanocrystals in 1 liter of ethanol. YbPO₄ nanoparticles were prepared according to the recipe described in Ref. [15]. For this work, we use nanoparticles calcinated at 200 °C. 10 ml of this doping solution was injected two times in the tube maintained horizontally. Before the second injection, one hour was waited to allow the solvent to evaporate. After this doping step, a temperature up to 1800 °C was applied to sinter the porous layer. Finally, the tube was collapsed at a temperature of 2100 °C to form the preform. This temperature was measured with a pyrometer pointing on the outside of the silica tube. The temperature of the core layer could be lower due to the thickness of the tube, varying from 1.5 mm at the beginning of the fabrication (during the porous layer deposition) to almost 5 mm during the collapsing step. The refractive index difference between the core and the cladding has been measured with the 2600 preform analyzer from Photon Kinetics (USA). The refractive index profile of the preform is reported in Figure 1a. The central dip is a common artifact induced by the MCVD process. As this study mainly focused on the evolution of the YbPO₄ crystals, we did not tried to optimize the refractive index profile. The drawing of the fiber was performed at 1950 °C.

2.2. Characterization

Scanning electron microscopy (SEM) imaging and Energy-dispersive X-ray spectroscopy (EDX) analyses were performed with a Tescan Vega 3 XMU SEM (Tescan France, Fuveau, France) equipped with an X-MaxN 50 EDX detector (Oxford Instruments, Abingdon, U.K.) and with a JEOL JSM 6700F SEM. EDX data were processed with the Aztec software (version 3.2, Oxford Instruments). Prior to those observations and analyses, fibers and preform sample were carefully polished and mounted on a SEM stub with carbon tape and subsequently carbon coated. Transmission electron microscopy (TEM) analyses were performed on a FEI Tecnai G2 microscope, operating at 200kV and equipped with a STEM module coupled to an Oxford SDD XMax 80 EDX detector. The thin lamella observed was taken by FIB (FEI Helios 600 Nanolab) on a portion of a thermally cleaved fiber. A complementary 3D analysis by FIB/SEM tomography was achieved on a FEI Helios 450s dual beam microscope. For this study, SEM images were acquired at 1kV with a resolution of 4 nm and a distance between successive images of 5 nm. A confocal Raman microscope (inVia Qontor, Renishaw Gloucestershire, UK) using a 532 nm laser was used to measure the Raman spectra as in [15]

3. Results and discussion

Germanosilica glass preform with a core of ~0.8mm (Fig. 1b) was prepared using MCVD and solution doping technique was used to add YbPO₄ crystals in the soot prior to collapsing the preform. While the initial size of the YbPO₄ crystals is less than 10 nm [15], they aggregate when they are suspended in solution as evidenced by the SEM image of the YbPO₄ crystals in Fig 5a obtained by letting a drop of the doping solution dry on a SEM stub. After the collapsing step, the preform was translucent. A cross-section of the preform was cut and polished to investigate the impact of the MCVD process on the survival of the YbPO₄ crystals. As shown in Fig. 1b, the composition of the core is not homogeneous. Particles are mainly observed in the whiter ring (Fig. 2a). Bright spots can be seen and according to the elemental mapping can be assumed to be YbPO₄ crystals (Fig. 2b-2e). From the elemental mapping, no YbPO₄ crystals are detected at the center of the core of the preform. The presence of the YbPO₄ crystals was confirmed using Raman

spectroscopy. The Raman spectra of the core and of the YbPO_4 crystals are shown in Fig. 3a. The Raman spectrum of the core exhibits broad bands at 400, 600, 800 and 1200 cm^{-1} which are typical bands of the different vibration modes of the silica glass network [18-19] and also sharp peaks at 1004 and 1065 cm^{-1} which can also be seen in the Raman spectrum of the YbPO_4 crystal [15]. However, the bandwidth of these peaks corresponds to that of the crystals after a calcination step at 1500 $^\circ\text{C}$ suggesting that the MCVD process improves the crystallinity of the initial doping crystals calcinated at 200 $^\circ\text{C}$ [15]. Figure 1d shows the mapping of the Raman signal at 1004 cm^{-1} measured in the center of the core and confirms the lack of the YbPO_4 crystals in the center of the core of the preform. However, when the preform is drawn into fiber, particles are observed in the center (Fig. 4)

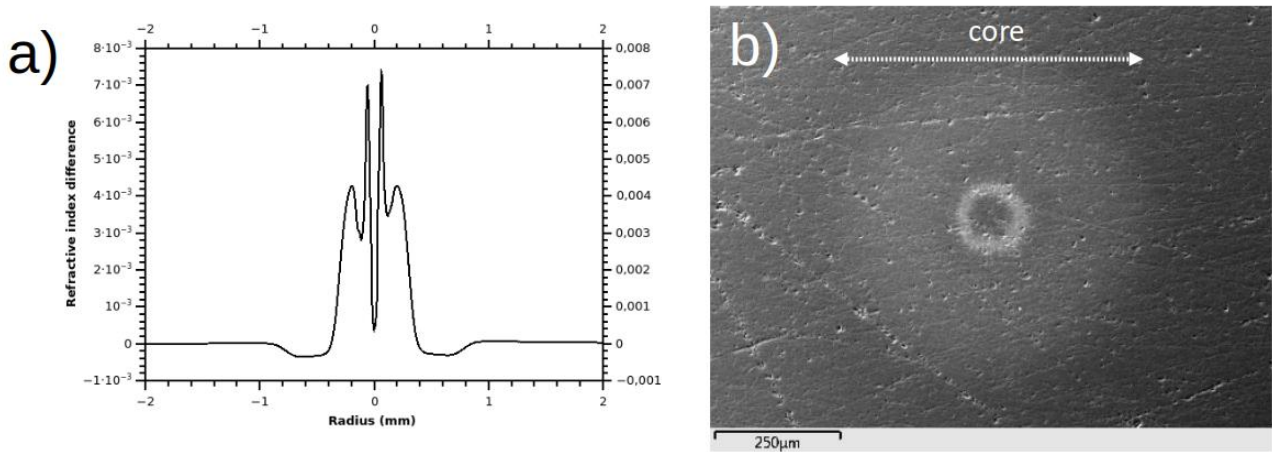


Figure 1: Refractive index profile of the preform (a) and SEM image of the preform (b).

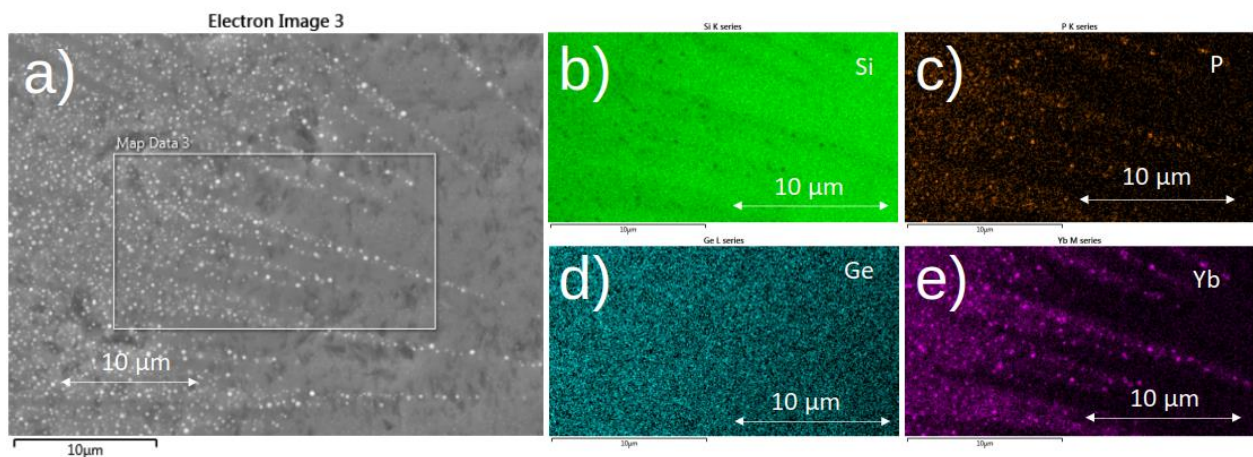


Figure 2: shows the SEM center measured in the white ring seen in the core of the preform with the elemental mapping of Si, Ge, P and Yb.

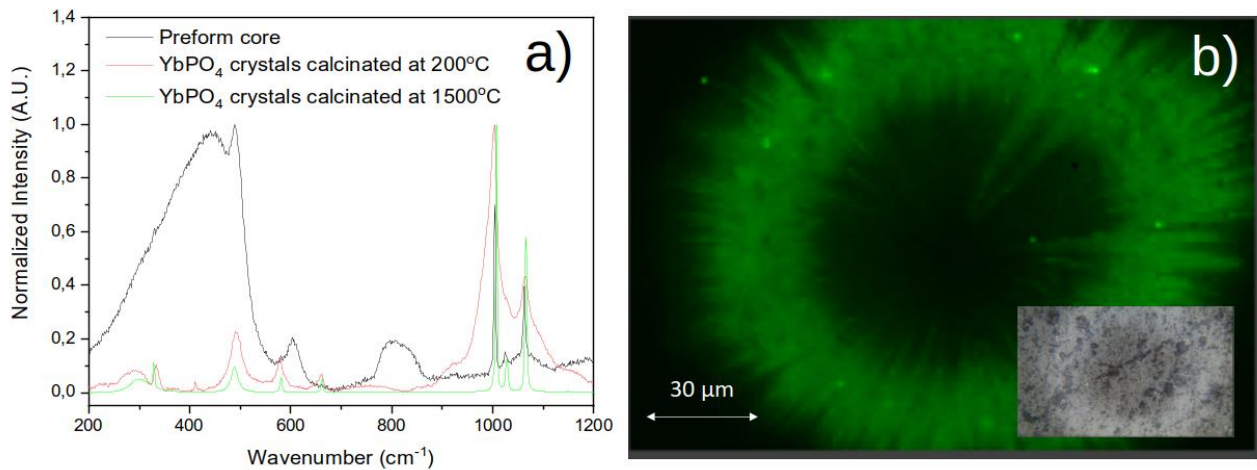


Figure 3: Raman spectra measured in the core of the preform and of the YbPO_4 crystals after calcination at 200 °C and 1500 °C (a) and the intensity mapping of the Raman signal centered at 1004 cm^{-1} (b)

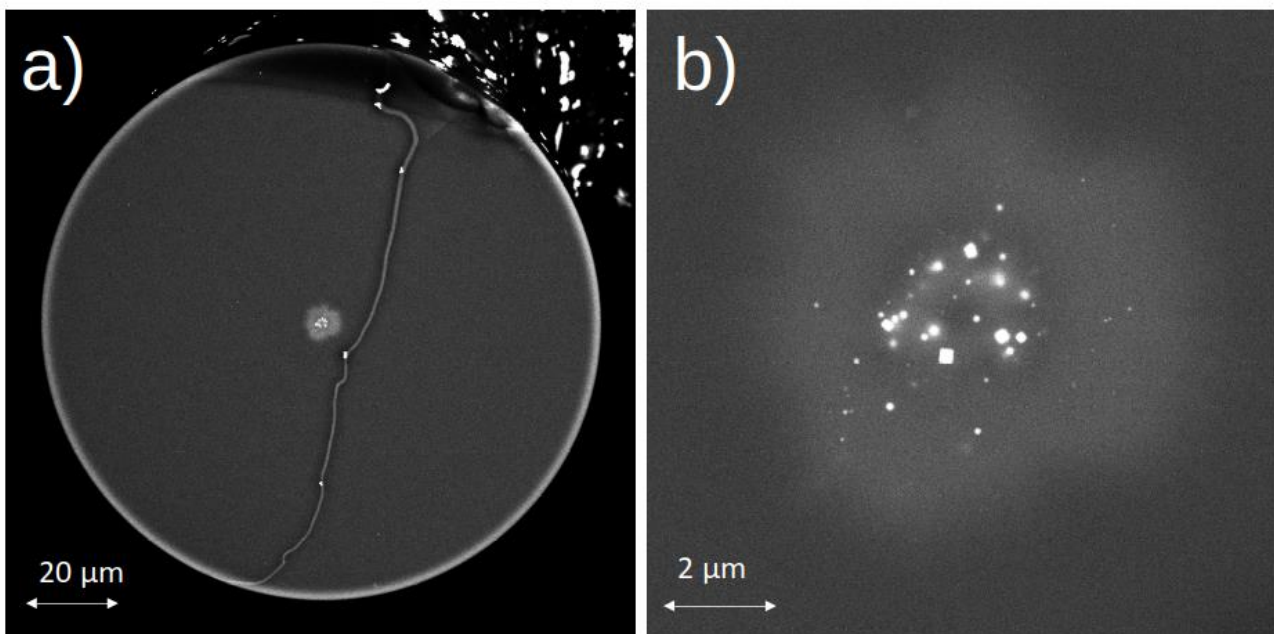


Figure 4: SEM images of the fiber, with (b) a close-up on the core

The homogeneous distribution of the crystals in the preform is evidenced in Fig. 5b which depicts the SEM image collected from a transverse section of the preform. From the SEM and Raman spectra analyses, there is no doubt that YbPO_4 crystals are present after the MCVD process. After collapsing, the preform was drawn into fiber. The fiber exhibits similar SEM images when measured in the cross section (Fig. 4b) and in a longitudinal section (Fig. 5e) than the preform. The longitudinal section of the elongated preforms and fiber along the drawing axis were analyzed as particles may elongate during the drawing step as suggested in [20]. Here, no evidence of such elongation nor breakup of the particles in the fiber is observed. It is then expected that all along the fabrication process, these particles have limited evolution. Particles size distributions have been estimated based on the SEM images taken at the same magnification, i.e. x5000 (Figure 5 b-e). On these images, particles of diameter below 3 pixels / 57 nm could not be measured. Particles size distributions looks very similar for all the steps in the fabrication of the fibers: preform of 10 mm (Fig. 5b) to elongated preform to 3 mm (Fig. 5c), to 1 mm (Fig. 5d) and finally to

fiber of a diameter of 125 μm (Fig. 5e). Particles with average size of about 100 nm can be seen in all samples (Figure 5f-i) despite the decrease of the diameter of the fiber by 2 orders of magnitude. These large particles present an irregular shape (some looks squared) which are typical of a crystalline structure.

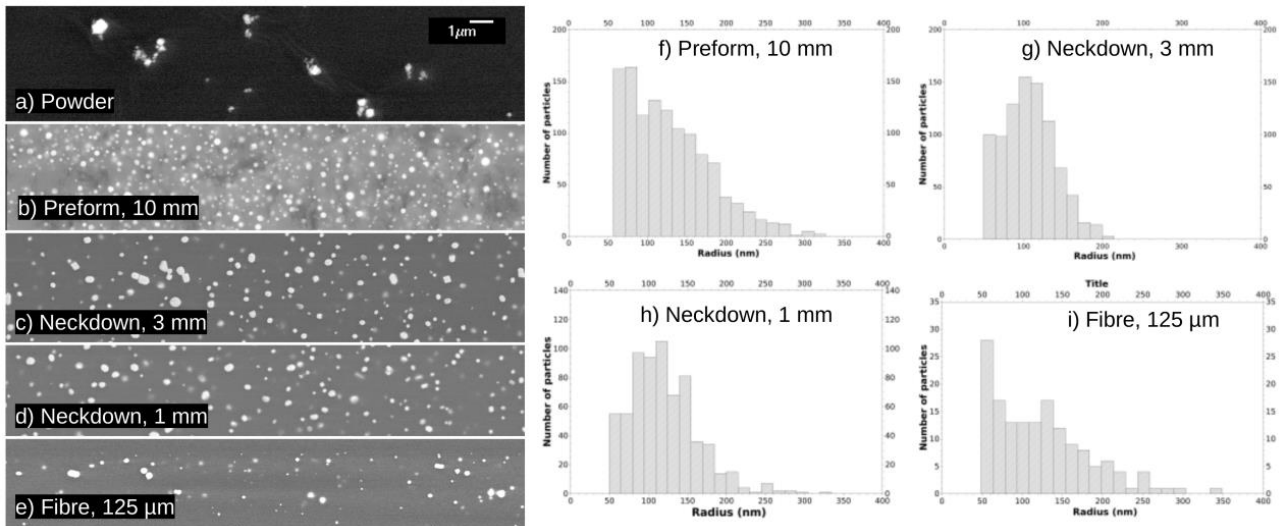


Figure 5 : SEM images of the (a) powder, (b) preform, (c,d) neckdown and (e) fiber core and the corresponding size distributions of the (f) preform, (g,h) neckdowns and (i) fiber. Fiber and neckdown samples were polished in the longitudinal direction (along the drawing axis) with a small angle of 3° . Preform sample was polished in the transverse section. All images have the same scale bar.

To determine the average fiber core composition, SEM/EDX data were acquired on a $2.5 \mu\text{m} \times 2.5 \mu\text{m}$ squared zone located at center of the core for three pieces of fibers. Ge, P and Yb concentrations were estimated to be 1.3, 0.4 and 0.4 at% (4.3, 0.55 and 3 wt%), respectively. In order to confirm the composition and the structure of the particles in the fiber, electron microscopy techniques were implemented. In Fig. 6a a particle is observed along a zone axis $\langle 100 \rangle$. The corresponding selected area electron diffraction pattern (Fig. 6b) is coherently indexed according to the xenotime phase of YbPO_4 . The particle shows the $\{020\}$ and $\{011\}$ facets. By tilting the sample by about 45° (Fig. 6c) the same particle is observed close to a $\langle 101 \rangle$ zone axis. Two new facets of type $\{101\}$ are now visible. These observations lead us to the conclusion that the real 3D shape of the particle corresponds to the combination of a tetragonal prism with a square bipyramid (Fig. 6e). For the observed particle, the c -axis of the crystalline particle is almost parallel to the fiber axis.

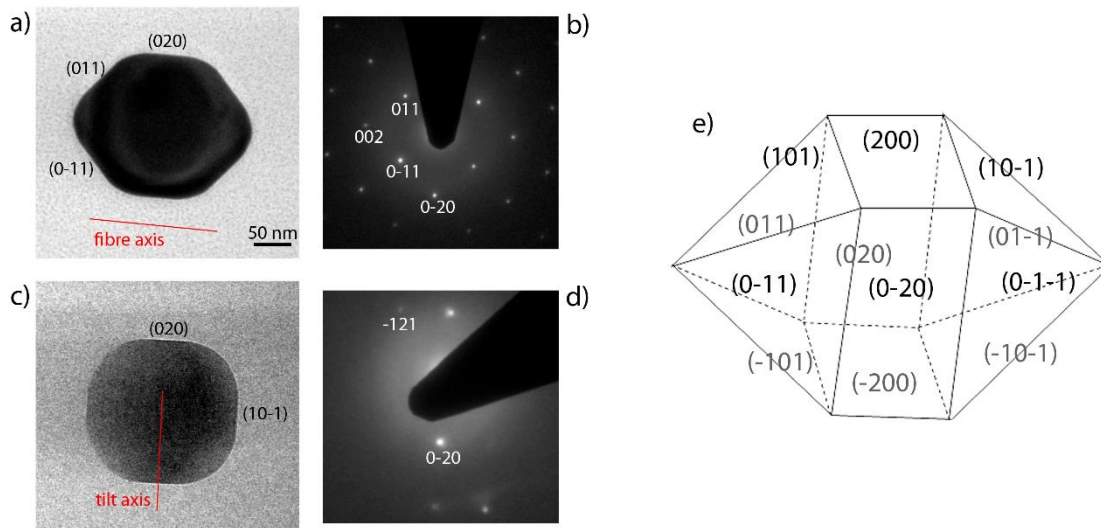


Figure 6 : TEM images of the same particle in $\langle 100 \rangle$ zone axis (a) and close to a $\langle 101 \rangle$ zone axis (c), and the corresponding SAED patterns (b) and (d). (e) Drawing of the particle shape.

In addition to this TEM analysis, a FIB/SEM study was carried out. The visualization of the 3D reconstruction is presented in Fig. 7. Only the particles contained entirely in the reconstructed volume are shown. The shape of the particles is in good agreement with the shape deduced from the TEM analysis. Looking at the particles in the x- and z-directions (Fig. 7), it appears that most of the particles have a c-axis oriented along the fiber axis (along y).

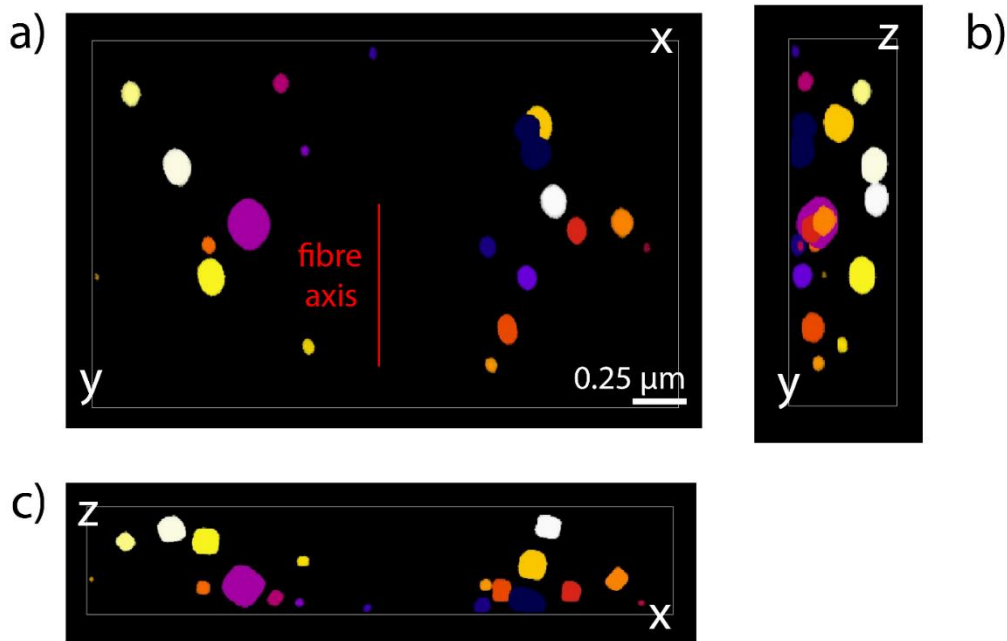


Figure 7: (a-c): 3D view of the reconstructed volume observed in z, x and y directions. Only the particles contained entirely within the reconstructed volume are shown.

EDX analyses were performed on a TEM specimen to determine the distribution of O, P, Si, Ge and Yb elements (Fig. 8). Based on these results, one can conclude that P and Yb elements are mainly present in the particles while Si and Ge elements are in the glass matrix. According to a

compositional analysis, the concentrations of Yb, P and O in the particles are 16, 17.2 and 66.9 at %, respectively, which is in excellent agreement with a YbPO_4 composition. The concentrations measured in the matrix, near the particles for O, P, Si and Ge are 66.7, 0.4, 31.6, 1.4 at %, respectively. For these quantifications, the concentration of oxygen was calculated by stoichiometry, assuming that it is bound by predefined stoichiometry to all other analyzable elements. The stoichiometry is defined by the valence of the oxygen ions and the valencies of other measured elements.

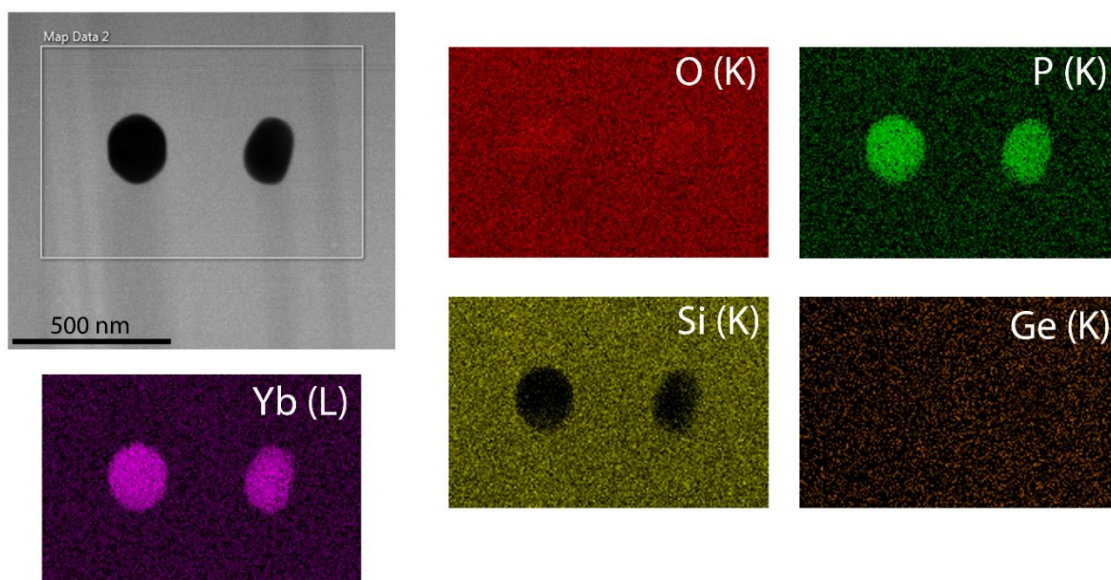


Figure 8 : STEM bright field image of particles (top left) and the corresponding EDX intensity maps for O, P, Si, Ge and Yb elements.

Conclusion

As a summary, it is demonstrated for the first time to the best of our knowledge that nanocrystals can be obtained directly in the as-drawn fiber, with the same composition and structure as the ones used as dopant. To reach this goal, YbPO_4 crystals were used as they are known to have high melting temperature (higher than the highest temperature used all along the fabrication process) and high chemical durability. Based on the SEM images, it seems that YbPO_4 crystals survive all along the process. However, it cannot be excluded that they partially melt and recrystallize. These results open new perspectives to fabricate glass-based composite fibers with controlled particle characteristics.

Declaration of Competing Interest

The authors declare that they have no known competing financial interests or personal relationships that could have appeared to influence the work reported in this paper.

Acknowledgements

CCMA electron microscopy equipment was funded by Région Sud - Provence-Alpes-Côte d'Azur, the Conseil Départemental des Alpes-Maritimes, and the GIS-IBISA. The Faculty of Engineering and Natural Sciences, Tampere University, is greatly acknowledged for the Doctoral Grant for NV.

References

- [1] W. Blanc, Z. Lu, T. Robine, F. Pigeonneau, C. Molardi, D. Tosi, Nanoparticles in optical fiber, issue and opportunity of light scattering, *Opt. Mat. Express* 12 (2022) 2635-2652.
- [2] D. Tosi, C. Molardi, M. Sypabekova, W. Blanc, Enhanced backscattering optical fiber distributed sensors: tutorial and review, *IEEE Sensors J.*, 21 (2020) 12667-12678.
- [3] A.G. Leal-Junior, D. Ribeiro, L.M. Avellar, M. Silveira, C.A.R. Díaz, A. Frizera-Neto, W. Blanc, E. Rocon, C. Marques, Wearable and fully-portable smart garment for mechanical perturbation detection with nanoparticles optical fibers. *IEEE Sens. J.*, 21 (2020) 2995-3003
- [4] B.N. Samson, P.A. Tick, N.F. Borrelli, N.F., Efficient neodymium-doped glass-ceramic fiber laser and amplifier. *Opt. Lett.* 26 (2001) 145-147
- [5] B.N. Samson, L.R. Pinckney, J. Wang, G.H. Beall, N.F. Borrelli, Nickel-doped nanocrystalline glass-ceramic fiber. *Opt. Lett.* 27 (2002) 1309-1311
- [6] W. Blanc, V. Mauroy, L. Nguyen, B.N. Shivakiran Bhaktha, P. Sebbah, B.P. Pal, B. Dussardier, B., Fabrication of rare earth-doped transparent glass ceramic optical fibers by modified chemical vapor deposition. *J. Am. Ceram. Soc.* 94 (2011) 2315-2318
- [7] Z. Fang, S. Zheng, W. Peng, H. Zhang, Z. Ma, S. Zhou, D. Chen, J. Qiu, Fabrication and Characterization of Glass-Ceramic Fiber-Containing Cr³⁺-Doped ZnAl₂O₄ Nanocrystals. *J. Am. Ceram. Soc.* 98 (2015) 2772–2775
- [8] P.A. Tick. Are low-loss glass–ceramic optical waveguides possible?. *Opt. Lett.* 23 (1998) 1904-1905
- [9] M. Henderson, B. Gibson, H. Ebendorff-Heidepriem, K. Kuan, S. Afshar V, J. Orwa, I. Aharonovich, S. Tomljenovic-Hanic, A. Greentree, S. Prawer, and T. Monroe. Diamond in tellurite glass: a new medium for quantum information. *Adv. Mater.* 23 (2011) 2806–2810
- [10] A. Pastouret, C. Gonnet, C. Collet, O. Cavani, E. Burov, C. Chaneac, A. Carton, J.P. Jolivet. Nanoparticle doping process for improved fibre amplifiers and lasers. In *Fiber lasers VI: technology, systems, and applications* (Vol. 7195, pp. 449-456) (2009). SPIE
- [11] M. Vermillac, H. Fneich, J.F. Lupi, J.B. Tissot, C. Kucera, P. Vennéguès, A. Mehdi, D.R. Neuville, J. Ballato, W. Blanc. Use of thulium-doped LaF₃ nanoparticles to lower the phonon energy of the thulium's environment in silica-based optical fibres. *Optical Materials*, 68 (2017) 24-28
- [12] N. Ojha, H. Nguyen, T. Laihinen, T. Salminen, M. Lastusaari, L. Petit. Decomposition of persistent luminescent microparticles in corrosive phosphate glass melt. *Corros. Sci.* 135 (2018) 207–214
- [13] A. Lemiere, A. Szczodra, S. Vuori, B. Bondzior, T. W. Hawkins, J. Ballato, M. Lastusaari, J. Massera, L. Petit. Bioactive phosphate glass-based fiber with green persistent luminescence. *Mat. Res. Bull.* 153 (2022) 111899.
- [14] C. Kinowski, H. El Hamzaoui, B. Capoen, G. Bouwmans, A.M. Blanchenet, K. Delplace, B. Prochet, M. Bouazaoui. YbPO₄ nano-cylinders formation and alignment within optical fiber preforms using fiber-drawing process. *Mat. Res. Bull.* 97 (2018) 293-299
- [15] A. Veber, T. Salminen, A. Matthes, R. Mueller, K. Wondraczek, L. Petit. Synthesis, characterization, and optical properties of ytterbium(III) phosphates and their incorporation in different glass matrices. *J. Phys. Chem. C* 125 (2021) 702–715
- [16] Y. Hikichi, T. Nomura, T. Melting Temperatures of Monazite and Xenotime. *J. Am. Ceram. Soc.*, 70 (1987) 252.
- [17] Y. Hikichi, T. Ota, K. Daimon, T. Hattori, M. Mizuno. Thermal, Mechanical, and Chemical Properties of Sintered Xenotime-Type RPO₄ (R = Y, Er, Yb, or Lu). *J. Am. Ceram. Soc.* 81 (1998) 2216–2218.

- [18] R.J. Bell, N.F. Bird, P. Dean. The vibrational spectra of vitreous silica, germania and beryllium fluoride. *J. Phys. C* 1 (1968) 299.
- [19] F.L. Galeener. Band limits and the vibrational spectra of tetrahedral glasses. *Phys. Rev. B* 19 (1979) 4292
- [20] M. Vermillac, J.F. Lupi, F. Peters, M. Cabie, P. Vennegues, C. Kucera, T. Neisius, J. Ballato, W. Blanc. Fiber-draw-induced elongation and break-up of particles inside the core of a silica-based optical fiber. *J. Am. Ceram. Soc.* 100 (2017) 1814-1819